UNIVERSITY OF CALIFORNIA

SANTA CRUZ

MODELING AND PREDICTION OF SINGLE-CELL GALVANOTAXIS DYNAMICS USING MACHINE LEARNING

A thesis submitted in partial satisfaction
of the requirements for the degree of

MASTER OF SCIENCE

in

SCIENTIFIC COMPUTING AND APPLIED

MATHEMATICS

by

Brett Sargent

June 2021

The Thesis of Brett Sargent
is approved:

_____
Professor Marcella Gomez,
Chair

_____
Professor Hongyun Wang

_____
Professor Min Zhao

_____
Quentin Williams
Acting Vice Provost and Dean of Graduate Studies

TABLE OF CONTENTS

LIST OF FIGURES

LIST OF TABLES

Abstract

Modeling and Prediction of Single-Cell Galvanotaxis Dynamics Using Machine Learning

by

Brett Sargent

It has long been known that many types of cells migrate in response to naturally-generated electric fields, and it has been suggested that the external application of an electric field may be used to intervene in and optimize natural processes such as wound healing. Precise cell guidance suitable for such optimization may rely on predictive models of cell migration, which are yet to be developed. Here, we present a deep learning model that can make predictions about the future directedness of cells given a timeseries of previous directedness and electric field values. This model can accept arbitrary electric field values, and we demonstrate that it can be used to perform *in silico* studies by simulating cell migration lines. Additionally, we show that our modeling approach can be used for a variety of cell types and experimental conditions with very limited training data using transfer learning methods. This predictive approach provides accurate models of cell migration which are suitable for use in control mechanisms with applications in precision medicine.

ACKNOWLEDGEMENTS

I would like to start by thanking my committee for taking the time to read this thesis and provide important feedback to guide this work towards its final version. Your expertise was invaluable, and your help was much appreciated.

I would particularly like to express my most sincere appreciation to my advisor, Dr. Marcella Gomez, for working with me throughout the duration of the project and providing valuable input and guidance to my research.

I would also like to gratefully acknowledge of the research labs of Dr. Min Zhao and Dr. Rivkah Isseroff at the UC Davis Department of Dermatology for generously providing the galvanotaxis tracking datasets used in our models and for using their expert knowledge to provide valuable insight about the biological implications of my work. Along with Dr. Zhao and Dr. Isseroff, I would like to thank Dr. Abijeet Mehta, Dr. Yao-Hui Sun, and Dr. Hsinya Yang for sharing and explaining their research into galvanotaxis.

Finally, I would like to extend my deepest gratitude to Dr. Mohammad Jafari for his constant, instrumental support and mentorship throughout the entire research process. This project could never have been completed without your assistance, and I have learned a great deal from our meetings. Thank you.

INTRODUCTION

A great number cell types, which have various functions, have been shown to migrate directionally in response to an electric field (EF) in a process known as galvanotaxis (also known as electrotaxis) (Mehta et al., 2021; Robinson, 1985; Sun et al., 2013; Yang et al., 2013; Zhu et al., 2020). Galvanotaxis may play a key role in many biological phenomena which are of significant medical interest, including wound healing (Reid & Zhao, 2014; Tai et al., 2009), embryo development (Erickson & Nuccitelli, 1984; Weijer, 2009), and cancer metastasis (Pu et al., 2007; Zhu et al., 2020). It has been suggested that electric fields can be manipulated to guide these biological processes for purposes such as accelerating would healing (Ojingwa & Isseroff, 2003; Kai et al., 2017; Ashrafi et al., 2017) and suppressing metastasis (Stuelten et al., 2018). For these approaches, galvanotaxis is favorable to other modes of motility because electric fields are very easy to apply and control precisely compared to alternatives such as chemoattractants (Prescott et al., 2021).

Direct observation of cell migration *in vivo* is difficult, so, while there are some promising studies of galvanotaxis *in vivo* (Feng et al., 2017; Lin et al., 2008), these studies are uncommon and most galvanotaxis studies are done *in vitro* (Ryan et al., 2021). There has been a call for a standardization and automation of galvanotaxis experiments to allow for deeper investigation into galvanotactic processes (Ryan et al., 2021). In addition to standardization of experimental design, it would be advantageous to standardize and automate the modeling of the effects of galvanotaxis. The development of general data-driven galvanotaxis modeling techniques would

allow for automated analysis of arbitrary galvanotaxis experiments using standard cell tracking data. Such automated modeling could open the door to deeper understanding of the dynamics of galvanotaxis and be used in the development of bioelectric medicine applications.

Towards guiding cellular migration through the application of a synthetic electric field, it may be advantageous to use a time-varying electric field driven by an intelligent automatic controller rather than applying a constant electric field. Extended applications of electric fields can be detrimental to tissues, meaning that attempts to guide cells via external EFs would require designing dynamic EF signals to maximize the ratio of responsiveness to current. To this end, the development of accurate and robust predictive models of galvanotaxis is of paramount importance to efforts towards optimizing galvanotactic responses in order to control biological processes. While there have been many models of galvanotaxis (Akiyama et al., 2017; Ogawa et al., 2006, 2005; Vanegas-Acosta et al., 2012), there have been very few efforts to develop predictive models of single-cell galvanotactic dynamics (Prescott et al., 2021).

Cell migration is notoriously difficult to model because cells have complex nonlinear responses to numerous environmental cues (Lara Rodriguez & Schneider, 2013). In general, there are two standard modeling approaches which include mechanistic models and data-driven models. Mechanistic models of single-cell galvanotaxis are more informative about the driving processes behind motility induced by an EF, but they lack predictive ability. The current predictive models are

capable of replicating ground truth cellular behavior as well as revealing the contributions of various means by which EFs induce migration, but they are unable to adapt predictions to different EF values without retraining (Prescott et al., 2021). Our proposed neural network-based model does not itself provide insight into means and mechanisms of galvanotaxis, but allows for prediction of migration directedness in a wide variety of experimental conditions, making it suitable for application to intelligent automatic controllers for use in influencing complex biological processes.

In this paper, we propose a predictive deep learning-based approach to modeling EF-guided migration at the single-cell level. Our models utilize a long short-term memory (LSTM) recurrent neural network architecture, which have been shown to have great success in capturing temporal patterns for time series prediction tasks (Gers et al., 1999; Hochreiter & Schmidhuber, 1997; Hua et al., 2019). Our approach has several advantages over existing methods. First, our model accepts arbitrary EF strengths, and the predictive accuracy remains high when making predictions on EF values not encountered in training. Furthermore, our model accepts EF values which vary in time, allowing for predictions to be made in settings where EFs may not remain constant such as those where the EF is regulated by a feedback controller for directing cellular response. Next, our model is capable of using transfer learning methods to make accurate predictions on different cell types using limited training data. Finally, our model is capable of performing *in silico* galvanotaxis experiments with any choice of time-varying EF values through the generation of

synthetic directedness data. These simulations can be used to minimize and guide experiments.

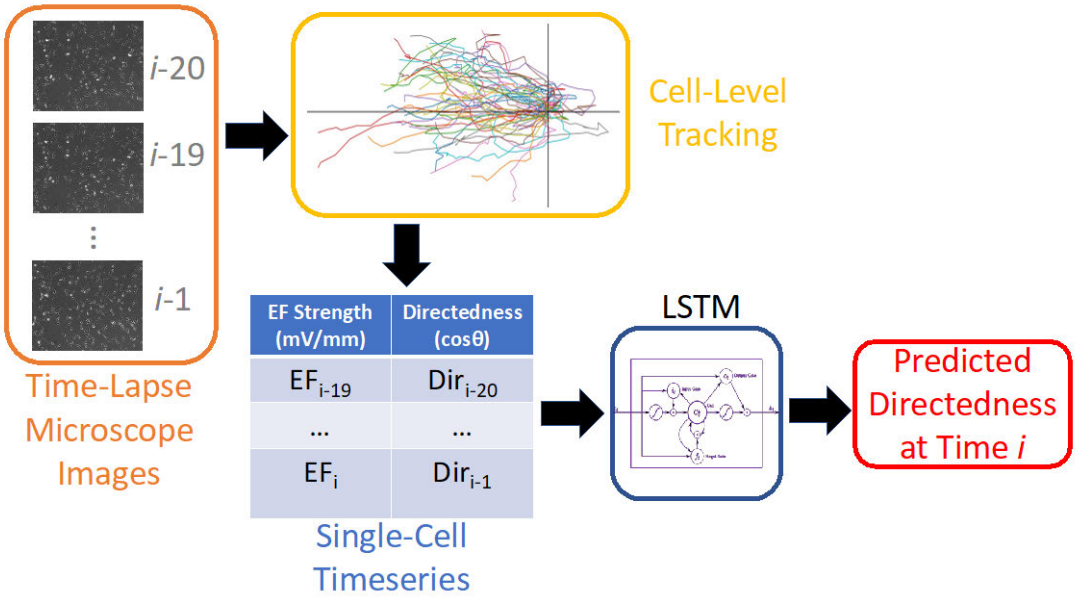

Figure 1: The image processing and cell directedness prediction pipeline. Time-lapse microscope images are used to manually track a number of cells. The tracking data is used to create timeseries of our two features, which are used as inputs to our blackbox LSTM model to make predictions about the next directedness value.

RESULTS

Recurrent NNs

We use a long short-term memory (LSTM) recurrent neural network to predict the future directedness (defined as the cosine of the angle between the electric field and the straight line which connects the start point of a cell and its current location) of a cell given its previous directedness and the current strength of the electric field. This is also referred to as a one-step ahead prediction. LSTM models have feedback

connections and are designed to explicitly avoid the vanishing gradient problem, meaning that they can process entire sequences of timeseries data (Hochreiter, 1998). LSTM networks are advantageous over other recurrent networks since they are relatively insensitive to the duration of time delays (Tian et al., 2021). These advantages make LSTM models desirable for understanding complex systems, and LSTM models have had success capturing the behavior of noisy dynamical systems (Yeo, 2019; Yeo & Melnyk, 2019).

Recurrent neural networks can predict the directedness of EF-induced cell migration at the single cell level

We first train and test the model on a collection of time-series data tracking single cell migration under a set of EFs: 0mV/mm, 15mV/mm, 30mV/mm, 50mV/mm, 75mV/mm, 100mV/mm, and 200mV/mm. To understand the generalizability of the model with respect to the EF strength, we then use the model to both interpolate and extrapolate to EF strengths that were not seen in the training set. For interpolation, we remove all instances of cells in an intermediate EF, 30mV/mm, from the training set and train a new model with identical architecture as before. For extrapolation, we follow a similar approach except we remove all instances of cells in an extreme EF, 200mV/mm from the training set. These models are then tested on the entire range of EFs. We also highlight the performance exclusively on cell trajectories under EFs omitted during training.

To evaluate the model's accuracy, we consider the distribution of root mean squared error (RMSE) values for single cell trajectories over a population of cells. In particular, we consider the median value and the inter-quartile range (IQR), which are 0.029 and 0.035, respectively, for the base model on the test set.

Figure 2 shows the results of predicting single-cell behavior for all EFs. The median RMSE values when predicting on the training and the test sets are 0.031 and 0.029, respectively. The IQR of RMSE distributions on the training and test sets are 0.033 and 0.035, respectively. The center and spread of the RMSE distributions for the training and test sets are comparable, showing that the model is not overfit. This is further supported by model simulations in a later section. The distributions of RMSE values when predicting on the training, validation, and test sets are shown in the following figure.

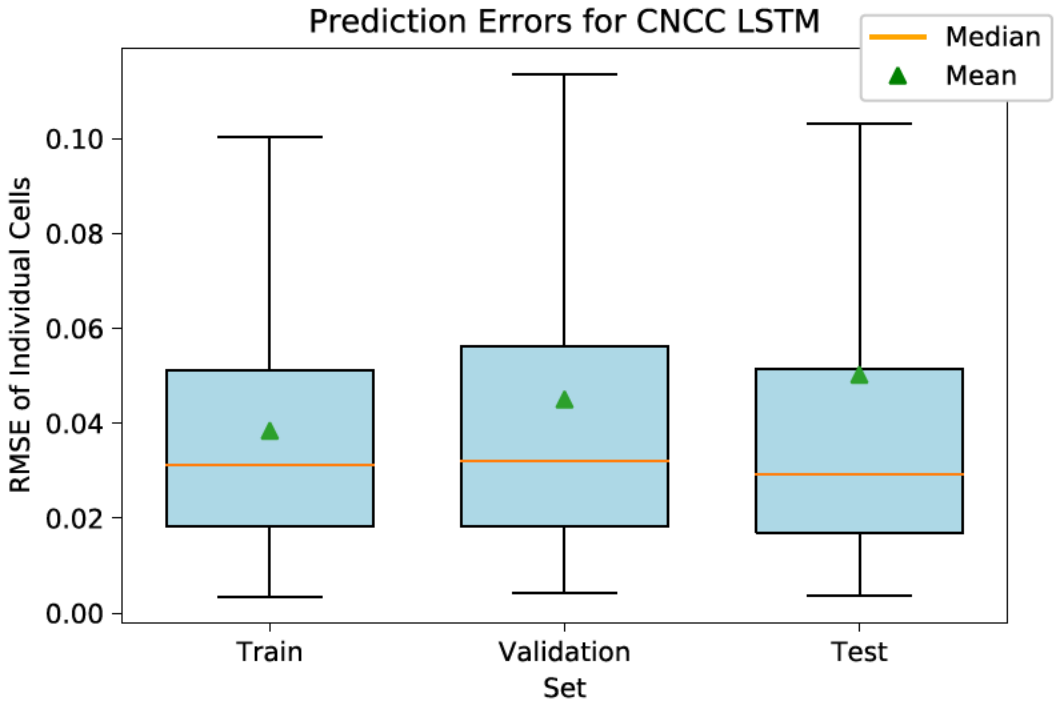

Figure 2: Distributions of cell-level root mean squared errors (RMSE) of the LSTM model on the training, validation, and test sets of CNCC tracking data.

Additionally, to demonstrate that the predictions are indeed informed we compare the results to those of two naïve predictors (see Figure 3). The first of these predictors, which we will call the "constant directedness" model for this discussion, makes a naïve assumption that directedness will remain constant from one timestep to the next. So, the directedness prediction made by this naïve model is just the previous directedness value. The second naïve predictor, which we refer to as the "linear" predictor, makes a linear extrapolation using the previous two directedness values. That is, the rate of change of directedness between the previous two timesteps is assumed to remain constant between the previous timestep and the next timestep. The median RMSE values for the constant directedness predictor and the linear predictor

are 0.169 and 0.198, respectively. The corresponding IQR values are 0.079 and 0.122. We compare the error distributions of the naïve predictors to that of our base model, the LSTM.

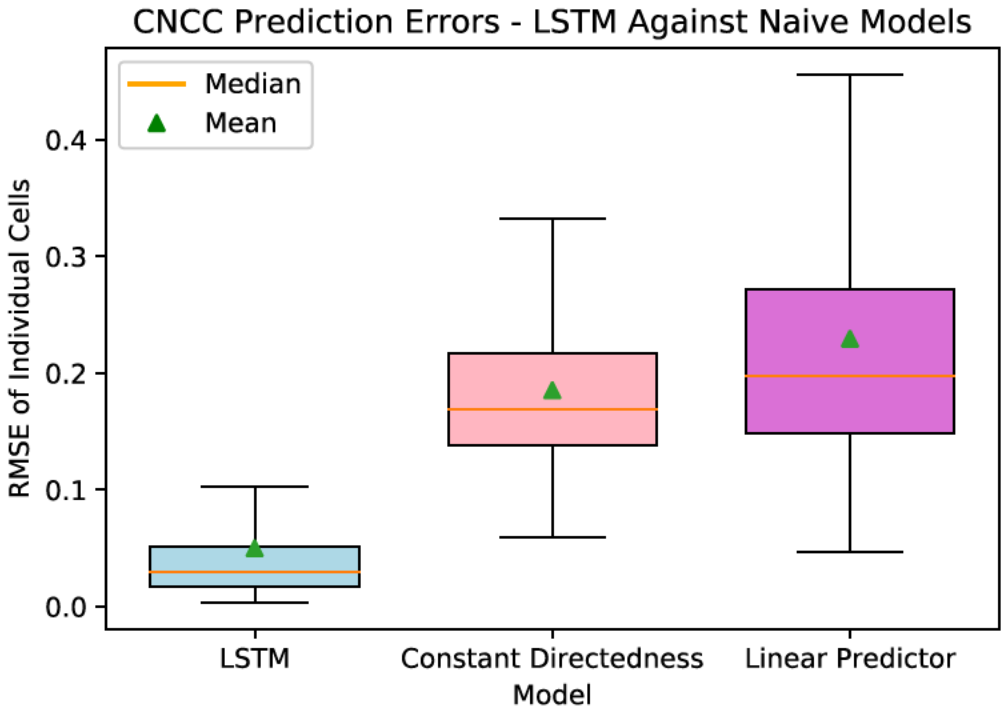

Figure 3: Distributions of cell-level test set RMSE values for our LSTM, a constant-directedness naïve model, and a linear predictor.

Next, we evaluate the ability of the model to interpolate to unseen EF strengths by considering the performance of a model trained without 30mV/mm instances on all cells in the test set, as well as on the 30mV/mm test instances (see Figure 4). On the full test set, the interpolation model has a median RMSE of 0.031, which is 5.48% higher than the base model, which was trained on the full training set. We evaluate the interpolation model specifically on the 30mV/mm test set instances, and the median RMSE value for these instances is 0.035. The median RMSE for the

original model is 0.034 on the 30mV/mm instances, which means that the increase in median error of the model trained without 30mV/mm instances is 4.12%. The increase in error on 30mV/mm instances when we omit that EF strength from the training set is no higher than the increase in error on the full training set. The omission of that strength removes information from the training set and decreases performance as a whole, but that reduction in error is not particularly bad for test instances with the omitted voltage, meaning that the model interpolates well to unseen EF strengths.

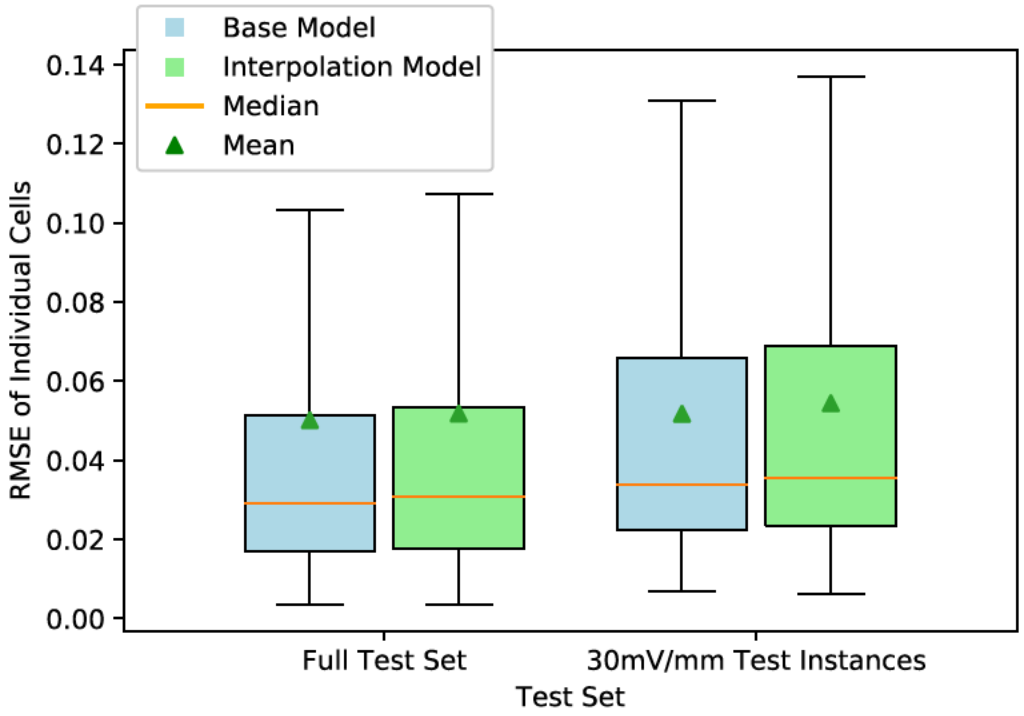

Figure 4: Distributions of cell-level test set RMSE values of the base model and a model with identical architecture which was trained with a modified training set from which the 30mV/mm instances were removed. Error distributions shown for both the complete testing set and for the 30mV/mm test instances.

For extrapolation, we compare the base model to a model trained without any 200mV/mm instances (see Figure 5). The median RMSE of this extrapolation model, when evaluated on the full test set, is 0.031, which is 6.51% higher than the model trained on the full training set. When evaluating this model specifically on the 200mV/mm the median RMSE is 0.022. The median RMSE for the base model is 0.018 on the 200mV/mm instances, so the median error on the 200mV/mm test instances is 17.40% higher than that of the base model. The performance of our model on this extrapolation evaluation appears worse than on the interpolation task, though we see an overall performance decrease caused by a reduction in the richness of the training set, much like we saw with the interpolation task. Thus, some of the difference in 200mV/mm instance median RMSE between the base model and the extrapolation model may be attributed to the error increase across the full test set caused by the limited training set.

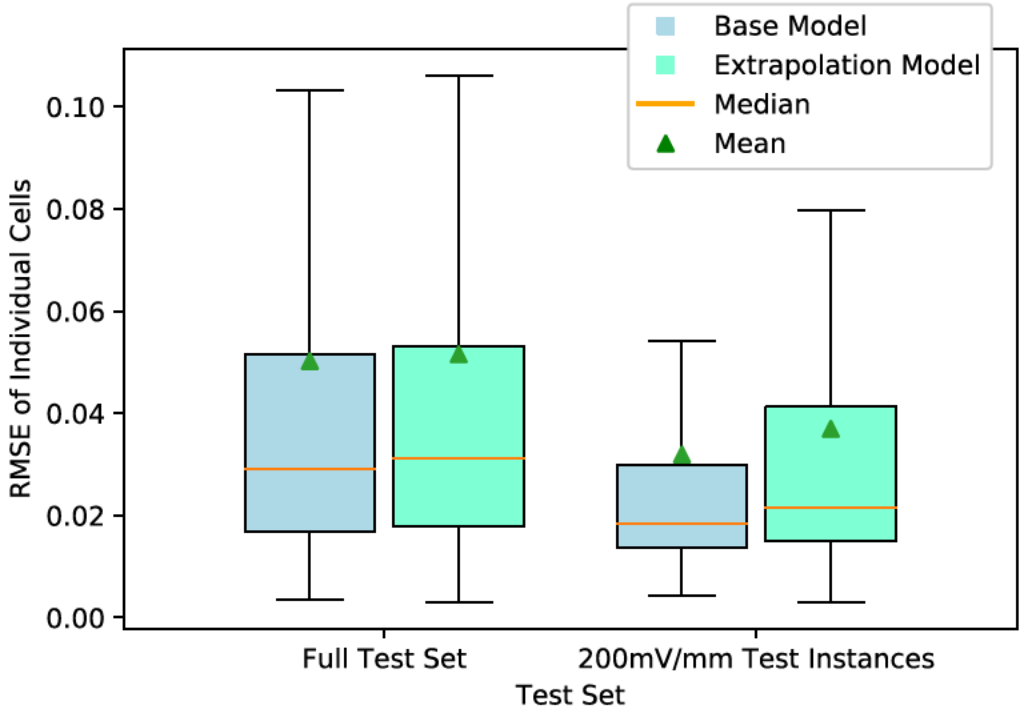

Figure 5: Distributions of cell-level test set RMSE values of the base model and a model with identical architecture which was trained with a modified training set from which the 200mV/mm instances were removed. Error distributions shown for both the complete testing set and for the 200mV/mm test instances.

For both the interpolation and extrapolation tests, the model trained on the limited training set performs worse than our original model overall. In the interpolation case, the increase in error is higher for the overall performance (5.48%) than it is for just the interpolated value (4.12%). For extrapolation, the increase in error is significantly higher for the instances with the extrapolated EF value (17.40%) than the increase in overall performance (6.51%), though the median RMSE on the 200mV/mm instances (0.022) remains fairly low when compared to the overall median RMSE (0.031). We expect the overall performance to decrease in both cases due to the limited number and variety of training instances, but the performance on

the missing values demonstrates the ability of our model to interpolate and extrapolate with respect to EF values, though our model seems to have relatively better performance on the interpolation task than on the extrapolation task.

Transfer learning allows for high prediction accuracy when minimal data is available

Transfer learning is the method of using a model's knowledge about one learning problem (called the source domain) to improve the performance on a second, related learning problem (called the target domain) (Bozinovski, 2020; Pan & Yang, 2010; Rosenstein et al., 2005; Torrey & Shavlik, 2010; Weiss et al., 2016). Transfer learning allows for target domain instances to be in a different feature space and have a different distribution than the instances in the source domain, which allows for relatively high performance when target domain data is too limited to allow for such performance were the model to be trained from scratch (Pan & Yang, 2010; Weiss et al., 2016). Because galvanotaxis experiments and manual cell tracking can be both expensive and time-consuming, galvanotaxis tracking datasets for some cell types may be limited in both the number of cells tracked and the variety of EF conditions in which experiments are conducted. Thus, transfer learning may be a pivotal tool in developing accurate models for cell types and experimental conditions for which data is limited. Here, we evaluate the effects of transfer learning on extending our constant EF CNCC model to different cell types and to a time-varying EF.

First, we consider transfer learning methods for making predictions on cells in time-varying EFs using the model which we trained on constant EFs. We evaluate the

ability of the model to capture CNCC galvanotaxis dynamics in an experiment in which the polarity of the EF is reversed halfway through the experiment (see Figure 6). We compare the performance of a "reversal model", trained only on the polarity reversal data, and a "transfer learning model", which retrains the base model on the polarity reversal data. We use the base model predictions on the constant-EF test set as a performance benchmark.

The median RMSE of the reversal model is 0.046, which is 57.20% higher than the benchmark performance of the base model on the original test set. The transfer learning model has a test set median RMSE of 0.038, which is an improvement of 18.09% over the reversal model. The transfer learning model's median test set RMSE is 28.77% higher than the benchmark model's median RMSE, which can likely be attributed to both the limited polarity reversal training data, as well as the increased complexity of dynamics in the time-varying EF setting. Despite the inability of the model to reach benchmark performance on this task, we have demonstrated that transfer learning methods are effective at improving model performance for cells in time-varying EFs over models trained only in those settings.

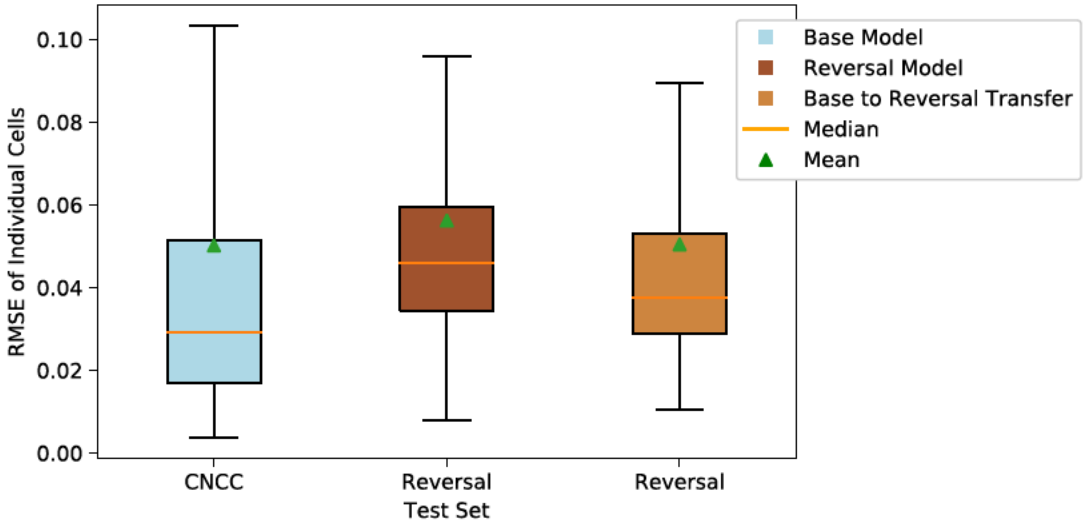

Figure 6: Distributions of cell-level test set RMSE values for our base model on the original test set (benchmark), the reversal model on the reversal test set, and the transfer learning model on the reversal test set.

Next, we evaluate the effectiveness of transfer learning methods for extending our method to cell types with limited galvanotaxis tracking data. We consider the application of our CNCC model to both fish keratocytes and human keratinocytes. Using limited training sets for both target cell types, we compare the performance of a model that uses the same architecture as our original model but has been trained only on the target data with our CNCC model, which we have retrained using the same target data using transfer learning methods. Again, we use the performance of the CNCC model as a benchmark, as our goal is that these models, once transfer learning methods have been applied, will have target data test performance similar to the benchmark test performance on the CNCC data.

We have one keratocyte dataset and three keratinocyte datasets. The keratocyte data contains tracking timeseries for 0mV/mm, 50mV/mm, 100mV/mm,

200mV/mm, and 400mV/mm electric fields. All keratinocyte cells are tracked in 100mV/mm EFs. The keratocyte training set contains tracking data for two cells from each available EF strength and the three keratinocyte training sets each contain tracking data for two cells total. For keratocytes, images are taken and cell positions are recorded every minute. The first two keratinocyte datasets also record positions at one-minute intervals, while the third keratinocyte dataset has positions recorded at ten-minute intervals. Thus, this task evaluates not only the ability of the model to transfer knowledge to other cell types, but also the ability of the model to adjust to different time delays.

Our keratocyte model, trained only on the keratocyte data, has a median RMSE of 0.055 on the test set, which is 89.73% higher than the median RMSE of the benchmark model performance on the CNCC test set. For transfer learning, we take the CNCC model and retrain the weights on the keratocyte training set, resulting in a median RMSE of 0.026 on the keratocyte test set, which is 53.07% lower than the keratocyte model which did not use transfer learning and 10.96% lower than the benchmark performance on the CNCC dataset. So, the model trained only on our limited keratocyte data has much higher median RMSE than the benchmark, while the transfer learning model achieves lower median error than the benchmark (see Figure 7).

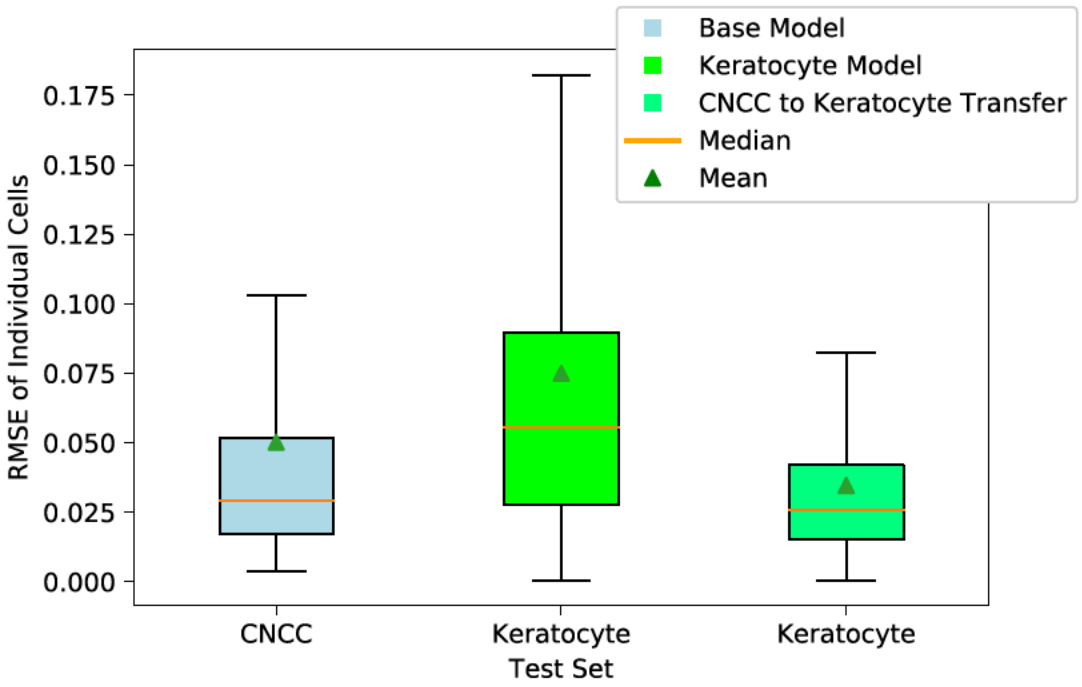

Figure 7: Distributions of RMSE values for the base model on the CNCC test set (benchmark), the keratocyte model on the keratocyte test set, and the transfer learning model on the keratocyte test set.

The first keratinocyte model, the model trained only on the first keratinocyte dataset, has a median RMSE of 0.101, 244.52% higher than the benchmark median RMSE. The transfer learning model, in which the base model was retrained using the same keratinocyte training set, has a test set median RMSE of 0.036, which is 64.02% lower than the median error of the model only trained on the keratinocytes, and is just 23.98% higher than the median RMSE of the benchmark CNCC model. The spread of the error distribution was also much lower for the transfer learning model than for the first keratinocyte model, with a RMSE IQR of 0.027 for the transfer learning model and 0.250 for the regular keratinocyte model (see Figure 8).

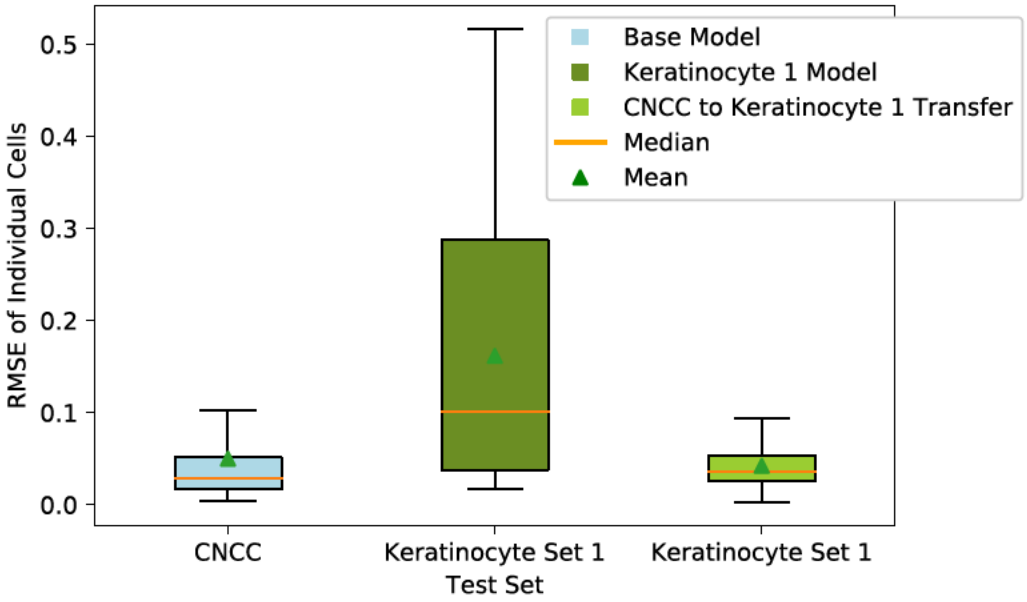

Figure 8: Distributions of RMSE values for the base model on the CNCC test set (benchmark), the keratinocyte 1 model on the keratinocyte 1 test set, and the transfer learning model on the keratinocyte 1 test set.

The median RMSE of the second keratinocyte model when predicting on the test set is 0.091, which is 210.96% higher than the benchmark median RMSE. After retraining the CNCC model on the second keratinocyte training set, the resulting model has a median RMSE of 0.067, which is 129.80% higher than the benchmark model, but 26.10% lower than the keratinocyte model that did not use transfer learning. Additionally, the distribution of errors has a much larger RMSE IQR for the second keratinocyte model (0.150) than for the associated transfer learning model (0.055) (see Figure 9).

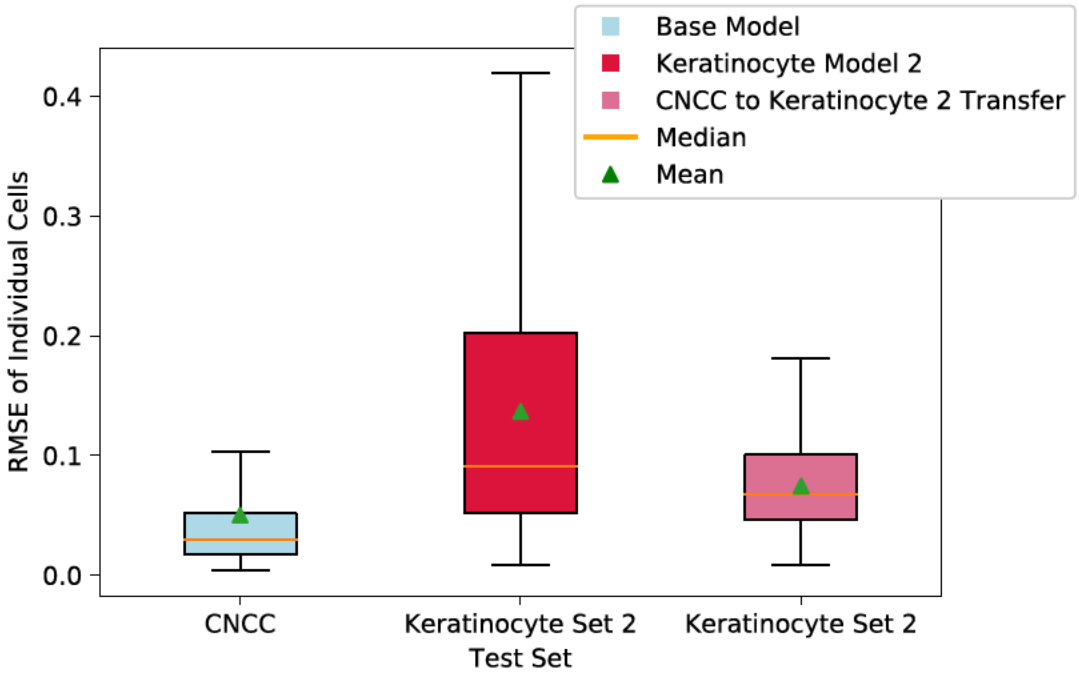

Figure 9: Distributions of RMSE values for the base model on the CNCC test set (benchmark), the keratinocyte 2 model on the keratinocyte 2 test set, and the transfer learning model on the keratinocyte 2 test set.

The median RMSE of the model trained only on the third keratinocyte dataset when predicting on the test set is 0.218, which is 645.21% higher than the benchmark median RMSE. After retraining the CNCC model on the third keratinocyte training set, the resulting model has a median RMSE of 0.113, which is 288.36% higher than the benchmark model, but 47.89% lower than the third keratinocyte model that did not use transfer learning. Once again, the spread is significantly lower in the model that used transfer learning, with a RMSE IQR of 0.106 in the transfer learning model and 0.238 in the regular third keratinocyte model (see Figure 10).

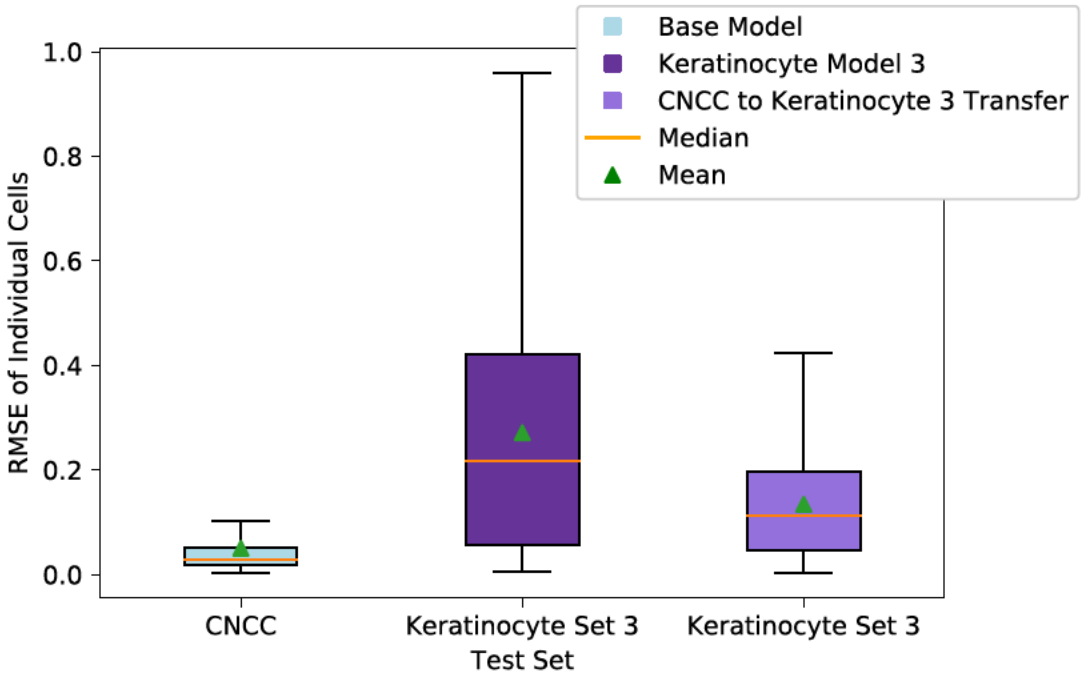

Figure 10: Distributions of RMSE values for the base model on the CNCC test set (benchmark), the keratinocyte 3 model on the keratinocyte 3 test set, and the transfer learning model on the keratinocyte 3 test set.

While transfer learning in these cases did not always lead to performance comparable to the benchmark, both the median and IQR of RMSE distributions were much lower for the transfer learning model than for the model trained only on the target cell type in all cases. We have shown that transfer learning can be an effective approach for developing predictive models about cell types for which available data is limited, even when the source cell data differs from target cell data in significant ways, such as the time interval between observations and anodal- versus cathodal-directed migration.

NN-based models can be used for *in silico* studies

In recent years, the massive increase in the quantity of available data has led to much attention being paid to *in silico* biological studies, which are studies performed on computers using mathematical modeling and simulations (Di Ventura et al., 2006; Palsson, 2000, 2002; Terstappen & Reggiani, 2001). The advantages of *in silico* studies include estimating hidden system parameters that are experimentally inaccessible (Kollmann & Sourjik, 2007), optimizing the timeline of experimental procedures and product development (Mancini et al., 2018; Silva et al., 2019), reducing the need for animal and human trials (Mancini et al., 2018), and lowering experimental costs (Jean-Quartier et al., 2018; Mancini et al., 2018; Silva et al., 2019). In this section, we demonstrate that the recurrent neural network-based model that we have developed can be used for *in silico* galvanotaxis assays with arbitrary and potentially time-varying EFs.

We simulate cell migration experiments by designing an EF timeseries and using some initial ground truth data to begin making predictions. In this way, we can generate timeseries of synthetic galvanotaxis tracking data using arbitrary EF values, which may vary in time. We compare the distributions of synthetic directedness values with those from the ground truth data to evaluate the ability of the model to capture the long-term effects of EFs on CNCC.

The specific comparison we consider is between the distributions of the directedness values at the end of the experiments. Our simulations use 20 timesteps of initial ground truth data to begin making predictions and each CNCC is tracked in a

constant EF for 36 timesteps after the initial image. Thus, we are comparing how the ground truth directedness distribution evolves in the final 17 timesteps with the evolution predicted by the simulation in the same time period. The ground truth data we consider are the 350 cells in the test set. These cells are used for the initial lookback to begin the simulations and for the comparison with ground truth final directedness values.

To determine the ability of our model to replicate the effects of an EF on cell motility *in silico*, we compare the distribution of final directedness values of the *in silico* synthetic data against the ground truth data across all of the EF values in the CNCC dataset (see Figure 11 and Table 1). We compare the directedness values by EF to evaluate whether the model has learned the effects of various EF values on the cells. If the distributions of EF-level predicted directedness values are similar to those of the EF-level ground truth directedness values, we can conclude that the *in silico* studies capture the general migration behaviors of the CNCCs.

The means and medians of final directedness values computed by the simulations are closely correlated with the ground truth. The correlation coefficient between the means is R=0.991 and the between the medians is R=0.972. In general, the distributions of simulated and ground truth final directedness values get closer as EF strength increases and cell behavior becomes more predictable.

Specifically, there is a significant drop in the differences between both means and medians at 30mV/mm and higher, compared to 0mV/mm and 15mV/mm simulations. The threshold of response of CNCC to electric fields has been identified

as being in the range between 15mV/mm and 30mV/mm(Mehta et al., 2021), so we expect that the simulations will more closely reflect the ground truth in EF strengths above that threshold due to the largely stochastic behavior of cells below the threshold.

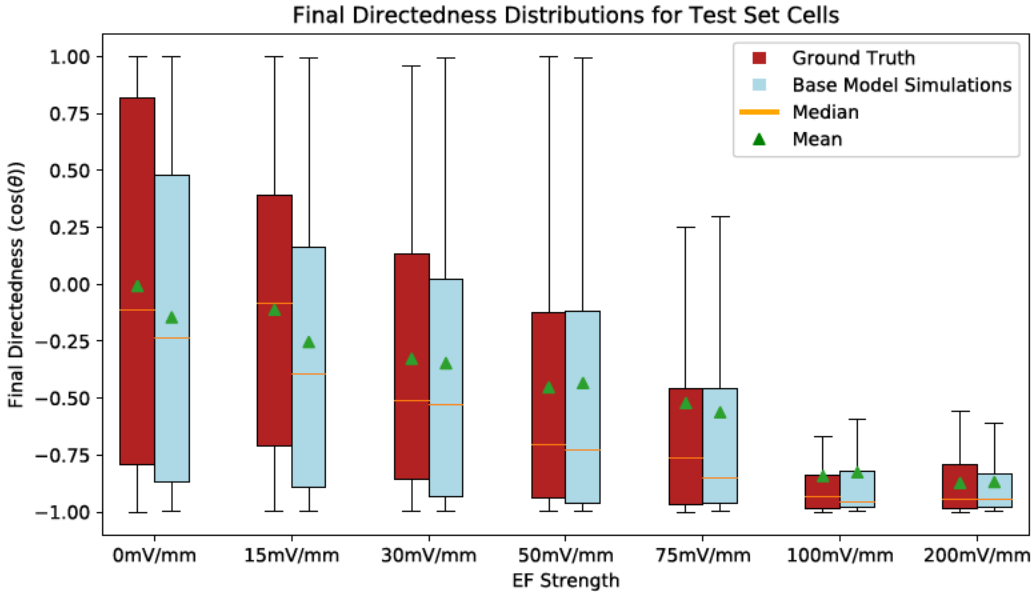

Figure 11: Distributions of final directedness values of cells in both ground truth data and synthetic data generated by simulations. For simulations, these distributions are over 50 trained models to ensure that these results are not dependent on the random initialization of any one model; see Methods subsection Recurrent Model Architecture for more details.

	0 mV/mm	15 mV/mm	30 mV/mm	50 mV/mm	75 mV/mm	100 mV/mm	200 mV/mm
Real Mean	-0.0071	-0.1114	-0.3266	-0.4520	-0.5210	-0.8416	-0.8718
Simulation Mean	-0.1455	-0.2531	-0.3462	-0.4333	-0.5617	-0.8260	-0.8683
Real Median	-0.1138	-0.0852	-0.5113	-0.7071	-0.7606	-0.9349	-0.9465
Simulation Median	-0.2381	-0.3920	-0.5317	-0.7298	-0.8511	-0.9531	-0.9463

Table 1: Means and medians of final directedness values for both ground truth and synthetic data. For simulations, these distributions are over 50 trained models to ensure that these results are not dependent on the random initialization of any one model; see Methods subsection Recurrent Model Architecture for more details.

DISCUSSION

Galvanotaxis has been observed in many cell types and plays key roles in processes such as wound healing and cancer metastasis. Here, we have presented a recurrent deep learning model which can capture the single-cell directedness dynamics of cranial neural crest cells. We have demonstrated that our deep learning model can make accurate predictions in constant-strength electric field settings even in EF strengths that were not seen by the model during the training stage, and that the model can simulate the effects of a time-varying EF. In addition, we have shown that the use of transfer learning methods can apply this model to different cell types, whose galvanotactic behavior is very different from the CNCC, to make predictions even when the data for the target cell type is scarce. There have been some previous

models of galvanotaxis (Vanegas-Acosta et al., 2012), and recently mathematical modeling has been used to quantify motility at a single-cell level (Prescott et al., 2021). However, to our knowledge, this work is the first to present a predictive deep learning model of single-cell motility, and the first model of any type to capture the response of cells to arbitrary EF strengths. Further, we are aware of no other work which has used the learned parameters from one cell type to aid in the modeling of other cell types.

An important advantage of the model we have presented is its ability to predict dynamics in a wide variety of experimental conditions due to its acceptance of arbitrary EF values, which may even vary in time. One of the potential applications of galvanotaxis models is informing controller-based intervention in wound healing and metastasis processes, and it is necessary for such models to be able to adapt to changing EFs without retraining, as external controllers may create significant fluctuations in EF strength. The ability of the model to both interpolate and extrapolate to new EF strengths and its performance the polarity switch experiment, along with the generation of qualitatively reasonable synthetic data, suggest that our model can make informative predictions about the behavioral response of cells to a wide variety of conditions.

Another key strength of this approach is the ability of our trained model to make reasonable predictions on other cell types after retraining on a very limited sample of the target cell data, even when the target cells exhibit vastly different electrotactic behavior from the original cell type. By training our model on a single

rich dataset, we can extend the model to a variety of cell types for which similarly rich datasets are unavailable. As galvanotaxis experiments and tracking procedures can be costly and time-consuming, the ability of our model to converge in the retraining stage for small datasets may allow for predictive models to be created with low experimental costs.

We have shown that our model is capable of driving simulations of cells which have similar galvanotactic behavior to those we see in our ground truth datasets. The value of these simulations is twofold. First, the similarities between the synthetic data generated by our model and the ground truth tracking data from real experiments illustrate that the predictions made by our model in response to various EF strengths are in line with how we expect real cells to behave given our dataset and literature on galvanotaxis tracking data. Second, these simulations demonstrate the potential for our recurrent models to perform *in silico* galvanotaxis migration experiments. Such experiments may be used in place of physical experiments, which would allow for reducing experimental costs and rapidly designing and implementing new experimental setups.

METHODS

Galvanotaxis Assay

The CNCC were isolated and cultured from the frontal and nasal bones of the cranial vault of neonatal wildtype C57BL/6 J mouse following established protocol

(Chen et al., 2020; Mehta et al., 2021; Wong & Cohn, 1975). Passage 3-5 of primary cells were used. The cells were loaded into the electrotactic chamber (pre-coated with 1:50 diluted Matrigel) and incubated for 4 hours to allow for attachment. Agar/saline bridges were placed into the chamber channels for application of DC electric field (Mehta et al., 2021).

For the keratocyte assay, scales were removed from the flanks of black skirt tetra and allowed to adhere to the bottom of a culture dish, where they were cultured at room temperature. Sheets of keratocytes that migrate off the scale after 24-48 hours were dissociated, seeded in tissue culture dish, and incubated at room temperature for 1-3 hours to allow for attachment. The galvanotaxis experiments were performed using custom-made electrotaxis chambers built over the tissue culture treated dishes (Sun et al., 2013).

The neonatal human keratinocytes (NHK) were isolated and cultured from foreskin, collected from elective circumcision surgeries under an IRB protocol approved by the UC Davis Institutional Review Board (IRB) Administration. NHK between passage 2-5 were plated on collagen coated galvanotaxis chambers at 6–8×10^4 cell/ml for 2 hours to allow the cells to attach and migrate. A 100 mV/mm DC electric field (EF), comparable to the physiological range at the wound field, was applied to the chambers for galvanotaxis (Yang et al., 2013).

Microscopic Imaging and Cell Tracking

For the CNCC, images were taken at 5-minute intervals for 180 minutes using an inverted microscope. The cells were tracked manually using ImageJ (National Institutes of Health) software (Mehta et al., 2021).

Keratocyte migration was recorded with a Zeiss Axiovert 40 with a Hamamtsu C4742-95 CCD digital camera attached. Images were taken at 1-minute intervals for up to two hours (Sun et al., 2013).

For the keratinocyte data, time-lapse Images (time interval of 1 minute for 60 minutes for the first two keratinocyte experiments and time interval of 10 minutes for 410 minutes for the third dataset) were acquired on a Nikon TE-2000 microscope with a motorized stage, an environmental chamber to maintain at 37°C, a 20× Nikon Plan Fluo objective, a Retiga EX camera (Qimaging, Canada), and the Volocity imaging software (PerkinElmer, Waltham, MA). Cell tracking was manually performed with OpenLab software and the cell migration rate and directionality of galvanotaxis were calculated (Yang et al., 2013).

Dataset Creation

Training and testing datasets were constructed using the cell position time series. For each cell position, the directedness is measured as the cosine of the angle between the EF and the straight line connecting the cell's current position with its starting position. While we typically discuss EF strengths as mV/mm because that is the SI unit for electric fields, the EF strength input to the model is in V/mm to put the

order of EF inputs on a similar order as the directedness values. At each timestep, our model uses the directedness and the EF strength. Because the LSTM has a 20 timestep lookback, each instance contains the 20 previous directedness values, the 19 previous EF values, and the next EF value (as features) along with the next directedness value (as the prediction target).

Recurrent Model Architecture

Our model was constructed and trained using Keras running on a TensorFlow backend. The model has a lookback of 20 timesteps and the data contains the directedness and EF strength at each timestep, so the input layer accepts matrices of shape (20,2).

Our primary model contains a single LSTM layer with 80 units which uses a hyperbolic tangent activation function and a sigmoid activation function for the recurrent step. The LSTM layer is densely connected to a single output unit using the hyperbolic tangent activation function.

The loss was measured as the square of the error and backpropagated through the network for each instance; that is, the batch size is 1 and the loss function is the squared error. To minimize prediction error, the loss was backpropagated through the network and weights were updated using the Adam optimizer with a learning rate of 0.001.

To ensure that the performance of our model is not an artifact of the random initialization of the weights, we train 50 versions of the model with identical

architecture and training procedure. The weights of each model are initialized randomly, and we consider the distributions of predictions over all 50 models, thus avoiding a reliance of our results on any particular initialization. When presenting results in the form of distributions of cell-level RMSE values, we calculate the RMSE for all predictions on a single cell for an individual model, and report all RMSE values from all models over all cells in the test set.

Implementation of Transfer Learning Methods

For the weight initialization transfer learning method which we use for predicting both, we begin by training the model on the CNCC training set (the source domain) and we then retrain the model on either the keratocyte dataset or the keratinocyte dataset (the target domains). The transfer learning method involves initializing the network weights as the optimal weights for the source domain before retraining all weights on the target domain. This method relies on the assumption that our time series forecasting task shares some similarities, despite the differences in galvanotaxis dynamics between different cell types. Thus, the weight configuration of the source domain model is assumed to be a better starting point for the learning process on the target domain data than a random initialization, allowing for the network to converge to an accurate predictive model in less time and with fewer training instances.

Generation of Synthetic Data

Because our model uses directedness and EF strength as input and predicts directedness, we can combine predicted directedness values with our choice of EF strength values to create synthetic input data which can in turn be fed back into the model to produce more directedness values. By using some initial lookback of ground truth experimental data to begin making predictions and some timeseries of EF values to combine with the predicted directedness values, we use our predictive model to simulate cell migration experiments of any length we wish. In this way, we can generate sequences of synthetic tracking data in which EF values are arbitrary and may vary in time.

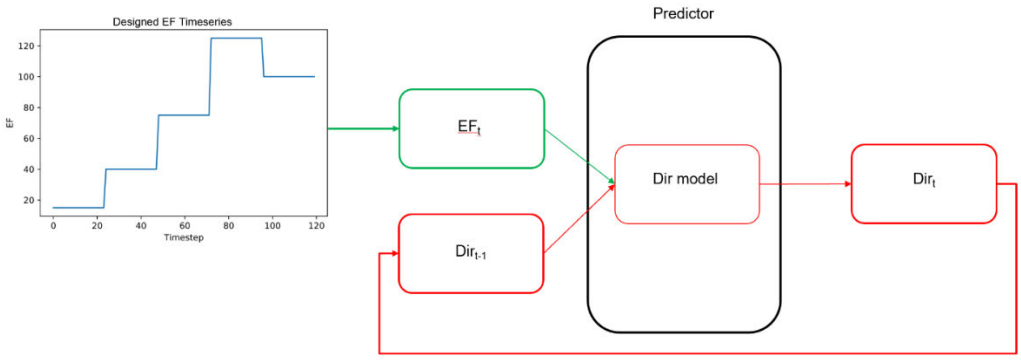

Figure 12: Diagram of simulation pipeline. An initial ground truth lookback is used to make a prediction, and that prediction is paired with an EF value from a designed timeseries. That predicted value is appended to the ground truth lookback and used as input to make another prediction. This process is repeated to generate more directedness values until the simulation is completed.

REFERENCES

Akiyama, M., Sushida, T., Ishida, S., & Haga, H. (2017). Mathematical model of collective cell migrations based on cell polarity. *Development, Growth & Differentiation*, *59*(5), 471–490. https://doi.org/10.1111/dgd.12381

Ashrafi, M., Alonso-Rasgado, T., Baguneid, M., & Bayat, A. (2017). The efficacy of electrical stimulation in lower extremity cutaneous wound healing: A systematic review. *Experimental Dermatology*, *26*(2), 171–178. https://doi.org/10.1111/exd.13179

Bozinovski, S. (2020). Reminder of the First Paper on Transfer Learning in Neural Networks, 1976. *Informatica*, *44*(3), Article 3. https://doi.org/10.31449/inf.v44i3.2828

Chen, X., Wang, H., Yu, M., Kim, J. K., Qi, H., Ha, P., Jiang, W., Chen, E., Luo, X., Needle, R. B., Baik, L., Yang, C., Shi, J., Kwak, J. H., Ting, K., Zhang, X., & Soo, C. (2020). Cumulative inactivation of Nell-1 in Wnt1 expressing cell lineages results in craniofacial skeletal hypoplasia and postnatal hydrocephalus. *Cell Death & Differentiation*, *27*(4), 1415–1430. https://doi.org/10.1038/s41418-019-0427-1

Di Ventura, B., Lemerle, C., Michalodimitrakis, K., & Serrano, L. (2006). From in vivo to in silico biology and back. *Nature*, *443*(7111), 527–533. https://doi.org/10.1038/nature05127

Erickson, C. A., & Nuccitelli, R. (1984). Embryonic fibroblast motility and orientation can be influenced by physiological electric fields. *Journal of Cell Biology*, *98*(1), 296–307. https://doi.org/10.1083/jcb.98.1.296

Feng, J.-F., Liu, J., Zhang, L., Jiang, J.-Y., Russell, M., Lyeth, B. G., Nolta, J. A., & Zhao, M. (2017). Electrical Guidance of Human Stem Cells in the Rat Brain. *Stem Cell Reports*, *9*(1), 177–189. https://doi.org/10.1016/j.stemcr.2017.05.035

Gers, F. A., Schmidhuber, J., & Cummins, F. (1999). *Learning to forget: Continual prediction with LSTM*. 850–855. https://doi.org/10.1049/cp:19991218

Hochreiter, S. (1998). *Recurrent Neural Net Learning and Vanishing Gradient*.

Hochreiter, S., & Schmidhuber, J. (1997). Long Short-Term Memory. *Neural Computation*, *9*(8), 1735–1780. https://doi.org/10.1162/neco.1997.9.8.1735

Hua, Y., Zhao, Z., Li, R., Chen, X., Liu, Z., & Zhang, H. (2019). Deep Learning with Long Short-Term Memory for Time Series Prediction. *IEEE Communications Magazine*, *57*(6), 114–119. https://doi.org/10.1109/MCOM.2019.1800155

Jean-Quartier, C., Jeanquartier, F., Jurisica, I., & Holzinger, A. (2018). In silico cancer research towards 3R. *BMC Cancer*, *18*(1), 408. https://doi.org/10.1186/s12885-018-4302-0

Kai, H., Yamauchi, T., Ogawa, Y., Tsubota, A., Magome, T., Miyake, T., Yamasaki, K., & Nishizawa, M. (2017). Accelerated Wound Healing on Skin by Electrical Stimulation with a Bioelectric Plaster. *Advanced Healthcare Materials*, *6*(22), 1700465. https://doi.org/10.1002/adhm.201700465

Kollmann, M., & Sourjik, V. (2007). In Silico Biology: From Simulation to Understanding. *Current Biology*, *17*(4), R132–R134. https://doi.org/10.1016/j.cub.2006.12.034

Lara Rodriguez, L., & Schneider, I. C. (2013). Directed cell migration in multi-cue environments. *Integrative Biology*, *5*(11), 1306–1323. https://doi.org/10.1039/c3ib40137e

Lin, F., Baldessari, F., Gyenge, C. C., Sato, T., Chambers, R. D., Santiago, J. G., & Butcher, E. C. (2008). Lymphocyte Electrotaxis in vitro and in vivo. *Journal of Immunology (Baltimore, Md. : 1950)*, *181*(4), 2465–2471.

Mancini, T., Mari, F., Massini, A., Melatti, I., Salvo, I., Sinisi, S., Tronci, E., Ehrig, R., Röblitz, S., & Leeners, B. (2018). Computing Personalised Treatments through In Silico Clinical Trials. A Case Study on Downregulation in Assisted Reproduction. *Intelligenza Artificiale*, 1–16. https://doi.org/10.29007/g864

Mehta, A. S., Ha, P., Zhu, K., Li, S., Ting, K., Soo, C., Zhang, X., & Zhao, M. (2021). Physiological electric fields induce directional migration of mammalian cranial neural crest cells. *Developmental Biology*, *471*, 97–105. https://doi.org/10.1016/j.ydbio.2020.12.011

Ogawa, N., Oku, H., Hashimoto, K., & Ishikawa, M. (2006). A physical model for galvanotaxis of Paramecium cell. *Journal of Theoretical Biology*, *242*(2), 314–328. https://doi.org/10.1016/j.jtbi.2006.02.021

Ogawa, N., Oku, H., Hashimoto, K., & Ishikawa, M. (2005). *Dynamics Model of Paramecium Galvanotaxis for Microrobotic Application*. *2005*, 1246–1251. https://doi.org/10.1109/ROBOT.2005.1570286

Ojingwa, J. C., & Isseroff, R. R. (2003). Electrical stimulation of wound healing. *The Journal of Investigative Dermatology*, *121*(1), 1–12. https://doi.org/10.1046/j.1523-1747.2003.12454.x

Palsson, B. (2000). The challenges of in silico biology. *Nature Biotechnology*, *18*(11), 1147–1150. https://doi.org/10.1038/81125

Palsson, B. (2002). In silico biology through "omics." *Nature Biotechnology*, *20*(7), 649–650. https://doi.org/10.1038/nbt0702-649

Pan, S. J., & Yang, Q. (2010). A Survey on Transfer Learning. *IEEE Transactions on Knowledge and Data Engineering*, *22*(10), 1345–1359. https://doi.org/10.1109/TKDE.2009.191

Prescott, T. P., Zhu, K., Zhao, M., & Baker, R. E. (2021). *Quantifying the impact of electric fields on single-cell motility* [Preprint]. Biophysics. https://doi.org/10.1101/2021.01.22.427762

Pu, J., McCaig, C. D., Cao, L., Zhao, Z., Segall, J. E., & Zhao, M. (2007). EGF receptor signalling is essential for electric-field-directed migration of breast cancer cells. *Journal of Cell Science*, *120*(19), 3395–3403. https://doi.org/10.1242/jcs.002774

Reid, B., & Zhao, M. (2014). The Electrical Response to Injury: Molecular Mechanisms and Wound Healing. *Advances in Wound Care*, *3*(2), 184–201. https://doi.org/10.1089/wound.2013.0442

Robinson, K. R. (1985). The responses of cells to electrical fields: A review. *The Journal of Cell Biology*, *101*(6), 2023–2027. https://doi.org/10.1083/jcb.101.6.2023

Rosenstein, M. T., Marx, Z., Kaelbling, L. P., & Dietterich, T. G. (2005). To transfer or not to transfer. *In NIPS'05 Workshop, Inductive Transfer: 10 Years Later*.

Ryan, C. N. M., Doulgkeroglou, M. N., & Zeugolis, D. I. (2021). Electric field stimulation for tissue engineering applications. *BMC Biomedical Engineering*, *3*(1), 1. https://doi.org/10.1186/s42490-020-00046-0

Silva, D. R., Sardi, J. de C. O., Freires, I. A., Silva, A. C. B., & Rosalen, P. L. (2019). In silico approaches for screening molecular targets in Candida albicans: A proteomic insight into drug discovery and development. *European Journal of Pharmacology*, *842*, 64–69. https://doi.org/10.1016/j.ejphar.2018.10.016

Stuelten, C. H., Parent, C. A., & Montell, D. J. (2018). Cell motility in cancer invasion and metastasis: Insights from simple model organisms. *Nature Reviews Cancer*, *18*(5), 296–312. https://doi.org/10.1038/nrc.2018.15

Sun, Y., Do, H., Gao, J., Zhao, R., Zhao, M., & Mogilner, A. (2013). Keratocyte fragments and cells utilize competing pathways to move in opposite directions in an electric field. *Current Biology: CB*, *23*(7), 569–574. https://doi.org/10.1016/j.cub.2013.02.026

Tai, G., Reid, B., Cao, L., & Zhao, M. (2009). Electrotaxis and Wound Healing: Experimental Methods to Study Electric Fields as a Directional Signal for Cell Migration. In T. Jin & D. Hereld (Eds.), *Chemotaxis: Methods and Protocols* (pp. 77–97). Humana Press. https://doi.org/10.1007/978-1-60761-198-1_5

Terstappen, G. C., & Reggiani, A. (2001). In silico research in drug discovery. *Trends in Pharmacological Sciences*, *22*(1), 23–26. https://doi.org/10.1016/S0165-6147(00)01584-4

Tian, B., Wang, G., Xu, Z., Zhang, Y., & Zhao, X. (2021). Communication delay compensation for string stability of CACC system using LSTM prediction. *Vehicular Communications*, *29*, 100333. https://doi.org/10.1016/j.vehcom.2021.100333

Torrey, L., & Shavlik, J. (2010). *Transfer Learning* [Chapter]. Handbook of Research on Machine Learning Applications and Trends: Algorithms, Methods, and Techniques; IGI Global. https://doi.org/10.4018/978-1-60566-766-9.ch011

Vanegas-Acosta, J. C., Garzón-Alvarado, D. A., & Zwamborn, A. P. M. (2012). Mathematical model of electrotaxis in osteoblastic cells. *Bioelectrochemistry*, *88*, 134–143. https://doi.org/10.1016/j.bioelechem.2012.08.002

Weijer, C. J. (2009). Collective cell migration in development. *Journal of Cell Science*, *122*(18), 3215–3223. https://doi.org/10.1242/jcs.036517

Weiss, K., Khoshgoftaar, T. M., & Wang, D. (2016). A survey of transfer learning. *Journal of Big Data*, *3*(1), 9. https://doi.org/10.1186/s40537-016-0043-6

Wong, G. L., & Cohn, D. V. (1975). Target cells in bone for parathormone and calcitonin are different: Enrichment for each cell type by sequential digestion of mouse calvaria and selective adhesion to polymeric surfaces. *Proceedings of the National Academy of Sciences*, *72*(8), 3167–3171. https://doi.org/10.1073/pnas.72.8.3167

Yang, H.-Y., Charles, R.-P., Hummler, E., Baines, D. L., & Isseroff, R. R. (2013). The epithelial sodium channel mediates the directionality of galvanotaxis in human keratinocytes. *Journal of Cell Science*, *126*(Pt 9), 1942–1951. https://doi.org/10.1242/jcs.113225

Yeo, K. (2019). Short note on the behavior of recurrent neural network for noisy dynamical system. *ArXiv:1904.05158 [Physics]*. http://arxiv.org/abs/1904.05158

Yeo, K., & Melnyk, I. (2019). Deep learning algorithm for data-driven simulation of noisy dynamical system. *Journal of Computational Physics*, *376*, 1212–1231. https://doi.org/10.1016/j.jcp.2018.10.024

Zhu, K., Hum, N. R., Reid, B., Sun, Q., Loots, G. G., & Zhao, M. (2020). Electric Fields at Breast Cancer and Cancer Cell Collective Galvanotaxis. *Scientific Reports*, *10*(1), 8712. https://doi.org/10.1038/s41598-020-65566-0